Earth and Planetary Science Letters 614 (2023) 118196

Contents lists available at ScienceDirect

Earth and Planetary Science Letters

journal homepage: www.elsevier.com/locate/epsl

Constraining the mechanisms of aeolian bedform formation on Mars through a global morphometric survey

David A. Vaz [a,*], Simone Silvestro [b,c], Matthew Chojnacki [d], David C.A. Silva [a]

[a] Centre for Earth and Space Research of the University of Coimbra, Observatório Geofísico e Astronómico da Universidade de Coimbra, Coimbra, Portugal
[b] INAF Osservatorio Astronomico di Capodimonte, Napoli, Italy
[c] SETI Institute, Carl Sagan Center, Mountain View, CA, USA
[d] Planetary Science Institute, Lakewood, CO, USA

ARTICLE INFO

Article history:
Received 16 January 2023
Received in revised form 27 March 2023
Accepted 28 April 2023
Available online 17 May 2023
Editor: J.P. Avouac

Dataset link: https://hirise-pds.lpl.arizona.edu/PDS/

Keywords:
large Martian ripples
transverse aeolian ridges
bedform wavelength
aeolian
Mars
remote sensing

ABSTRACT

Aeolian processes on Mars form a distinct class of meter-scale ripples, whose mechanisms of formation are debated. We present a global morphometric survey of Martian bedforms, adding relevant observational constraints to the ongoing debate. We compare our results with previous surveys, highlighting inconsistencies in data used in previous studies, namely for the bedforms located in the Tharsis highlands.

We show that the bedforms located in the Tharsis region form a distinct group, not akin to the large dark-toned ripples which cover dune fields elsewhere on the planet. Tharsis bedforms form unique patterns, present distinct thermophysical characteristics and have higher albedos, suggesting they are formed and/or covered by finer materials.

The relation between wavelength and atmospheric density derived from the new data is consistent with the predictions of a wind-drag mechanism, favoring the model that uses a saltation saturation length. Regardless of the mechanism that limits the size of bedforms, these results confirm the existence of a robust relationship between the wavelength of large ripples and atmospheric density (ripples' spacing increases with decreasing atmospheric density). This provides further support to the interpretation of paleoatmospheric conditions on Mars through the analysis of its aeolian sedimentary record.

1. Introduction

Martian dark dunes are covered by large ripple-like bedforms which are actively migrating under present-day atmospheric conditions (Silvestro et al., 2010; Bridges et al., 2012). These are metric-scale bedforms (~1-5 m spacing between crests, ~5-40 cm high) which can have symmetrical or asymmetrical profiles and sinuous or straight crests (Lapotre et al., 2018). In terrestrial aeolian environments with well-sorted sediments there are no obvious analogue bedforms in terms of scale, morphometry and dynamics (Silvestro et al., 2016; Vaz et al., 2017; Lapotre et al., 2018). Most notably, the meter-scale bedform are overlaid by centimeter-scale ripples, similar in scale and dynamics to impact ripples common on Earth (Bridges et al., 2012; Lapotre et al., 2016; Weitz et al., 2018). The coexistence of these two different scales of bedforms raised several questions. Namely, why do we have two scales of ripples on Mars and what are the mechanisms that control their sizes?

To explain orbital and ground-based observations of widespread aeolian activity (Silvestro et al., 2010, 2013; Bridges et al., 2012; Baker et al., 2022), transient low-flux transport regimes, that occur between impact threshold and fluid threshold speeds were invoked (Sullivan and Kok, 2017; Baker et al., 2018; Lapotre et al., 2018; Swann et al., 2020; Andreotti et al., 2021). Recent in situ observations by the Curiosity rover at Gale crater demonstrate that intermittent saltation is taking place, contributing to the migration of centimeter-scale ripples (Baker et al., 2018, 2022; Sullivan et al., 2022). In addition, wind tunnel experiments suggest that the size of impact ripples does not vary significantly with atmospheric density, maintaining their characteristic centimeter scale even in the low density conditions that exist on the surface of Mars (Andreotti et al., 2021). Therefore, all evidence shows that the size of centimeter scale ripples on Mars is controlled by the same impact-splash mechanism that produces terrestrial aeolian impact ripples.

In contrast, two hypotheses have been proposed to explain the origin of the meter-scale ripples. They have been interpreted: a) as arising from a hydrodynamic instability i.e., they are analogous to

* Corresponding author at: CITEUC - Observatório Geofísico e Astronómico da Universidade de Coimbra, Almas de Freire, 3040-004 Coimbra, Portugal.
E-mail address: davidvaz@uc.pt (D.A. Vaz).

https://doi.org/10.1016/j.epsl.2023.118196

fluid drag ripples typically found on terrestrial subaqueous environments (Lapotre et al., 2016; Duran Vinent et al., 2019; Lapotre et al., 2021); or b) as forming from the same impact-splash mechanism as terrestrial aeolian ripples (Sullivan and Kok, 2017; Sullivan et al., 2020). In the first hypothesis, the equilibrium wavelength of the large ripples is limited by a hydrodynamic anomaly (Lapotre et al., 2017; Duran Vinent et al., 2019), while in the second case ripple height (and consequently their wavelength) is controlled by the wind dynamic pressure at the bedforms crests, which is lower on Mars and would allow the growth of the bedforms (Sullivan et al., 2020). Lapotre et al. (2016, 2021) argued that in well sorted sand there is a clear wavelength gap between the two types of bedforms, inferring that two different mechanisms are limiting the size of the bedforms (impact-splash for the centimeter-scale ripples and fluid-drag for the meter-scale bedforms). In contrast, Sullivan et al. (2022) reported a continuum distribution of superimposed ripple wavelengths observed by the Curiosity rover at the "Sands of Forvie" sand sheet. They also reported the existence of granulometric segregation between the troughs and crests of large ripples (the same was reported in other areas by Gough et al., 2021) with coarser grains preferentially located on the crests of the larger bedforms — a common observation in terrestrial deserts (Bagnold, 1941). They interpreted these two characteristics as evidence that the meter-scale ripples are impact ripples rather than fluid-drag bedforms. An important aspect of the debate about the mechanism that sets the size of large ripples is the near-inverse relation observed between wavelength and atmospheric density at a global scale. This relation was initially hinted at by Lorenz et al. (2014) for the bedforms located across the high elevation Tharsis region, while Lapotre et al. (2016) extended the number of surveyed areas, focusing on sites where dark dunes are present. Based on this compilation, Lapotre et al. (2016) argued that the observed decrease in ripple wavelength with increasing atmospheric density is consistent with a fluid-drag origin. A view not shared by Lorenz (2020), which highlighted the different gradient of the model predictions and observational data (see Fig. 2 in Lorenz, 2020). Lapotre et al. (2021) revisited the same dataset proposing that when a saltation saturation length formulation is adopted (Duran Vinent et al., 2019), the fluid-drag mechanism provides a better fit to the data, particularly to the bedforms analyzed outside Tharsis.

Drag ripples wavelength scales according to $\lambda \propto \frac{\left(\frac{\mu}{\rho_f}\right)^{2/3} D^{1/6}}{(Rg)^{1/6} u_*^{1/3}}$ (Lapotre et al., 2017), where μ is the dynamic viscosity, ρ_f is the fluid density, D is grain diameter, g is the gravity acceleration and R is the submerged reduced density of the sediment ($\frac{\rho_s - \rho_f}{\rho_f}$). This relation predicts that bedform wavelength is strongly dependent on $\rho_f^{-2/3}$. Rubanenko et al. (2022) used an earlier version of the data presented in this study to show that the wavelength of large ripples and the minimum size of barchans on Mars follow a similar power-law exponent. In addition, they documented the existence of a wavelength gap between the meter-scale dark ripples and small barchans on Mars, arguing that both types of bedforms form by the same hydrodynamic instability.

The mechanisms that set the wavelength of impact ripples are less understood. Wind tunnel experiments show that the saturation wavelength on well sorted sediments increases linearly with friction velocity (Andreotti et al., 2006; Rasmussen et al., 2015; Cheng et al., 2018), and is thought to be limited by the height of the ripples (Bagnold, 1941; Manukyan and Prigozhin, 2009). Yet, in less well sorted sediments coarser particles form an armor layer on the crests, causing ripples to increase in height and consequently in wavelength (Sharp, 1963). Sullivan et al. (2020) argue that the wind dynamic pressure $WDP = \frac{1}{2}\rho_f u^2$ (u is the wind velocity) controls ripples height, with higher dynamic pressures removing particles from the crests and precluding the growth of the bedforms. Therefore, higher WDP should generate smaller ripples. In this case, if we assume a constant wind velocity the wavelength of impact ripples scales with $1/\rho_f$. Note that this assumption (constant wind speed at a global scale) may be problematic, as according to the equation WDP may be relatively more influenced by wind velocity than by density variations, which is the only factor addressed in previous studies as well as in this work. Nevertheless, both theories suggest an increase in wavelength when atmospheric density decreases.

Other questions not entirely settled in previous studies regard the nature of the bedforms located in the Tharsis region. Lapotre et al. (2016) noticed the morphologic and albedo discrepancies between the dark-toned ripples covering dunes and Tharsis bedforms that occur far from dunes as sheets. Nevertheless, they merged the two datasets to fit their wind-drag model, while in later works Tharsis and non-Tharsis bedforms were analyzed separately (Lorenz, 2020; Lapotre et al., 2021).

Here we focus on these unresolved issues, reviewing and expanding the observational dataset, analyzing the consistency of measurements, and testing the models that predict the size of large ripples on Mars as a function of atmospheric density.

2. Data and methodology

We use High-Resolution Imaging Science Experiment (HiRISE) images (0.25-0.5 m/pix, McEwen et al., 2007) to perform a global scale mapping and wavelength survey of meter-scale aeolian bedforms. Our survey covers the same 25 areas located in the Tharsis regions and analyzed by Lorenz et al. (2014), as well as the 11 areas reported in Lapotre et al. (2016) (Fig. 1). Furthermore, we expand the elevation coverage including 39 new areas where meter-scale bedforms are present covering dark-toned dunes or sand sheets (Fig. S1 and Table S1).

Previous surveys relied on the discrete manual measurements of crest-to-crest distances in randomly selected points (Lorenz et al., 2014; Lapotre et al., 2016). Alternative automated methods allow the systematic mapping of bedform crests producing a set of polylines (Vaz and Silvestro, 2014; Foroutan and Zimbelman, 2017). These outputs can be used to study bedforms' spatial variations and patterns, however when applied at a dune field scale they generate a large set of crestlines, requiring subsequent spatial integration/generalization (Vaz et al., 2017). Furthermore, given the high number of ripples that can be present on one image, the size of the output datasets may be of the same order of magnitude of the image itself (a few gigabits), which complicates the study of these bedforms at a global level. Here we address these limitations, applying a set of image processing and machine learning techniques which allow the mass automatic mapping of bedforms and the accurate measurement of their wavelengths (Fig. 2). We adapted the 2D Fast Fourier Transform approach introduced by Voulgaris and Morin (2008) to study seabed bedforms, implementing a multiscale scheme coupled with neural networks. This method allows the mapping and characterization of large ripples and transverse aeolian ridges (TARs) in a wide range of spatial scales and surface settings. See Supplementary material 1 - section S1 for a in depth description of the method and results validation.

The elevations used in this work are extracted from the MOLA MEGDR (Mission Experiment Gridded Data Records) for each site. This dataset represents elevations above the areoid with a spatial resolution of 463 m/pixel (Smith et al., 1999). The spatial centroids of the largest bedform patches mapped in each area are used as sampling points. To assess possible measurement bias, we are also comparing our elevations with values reported in previous studies. Note that Lorenz et al. (2014) mentions that their elevation data was derived from MOLA data, however they do not provide any other detail (e.g. specific sampling locations, reference datum or

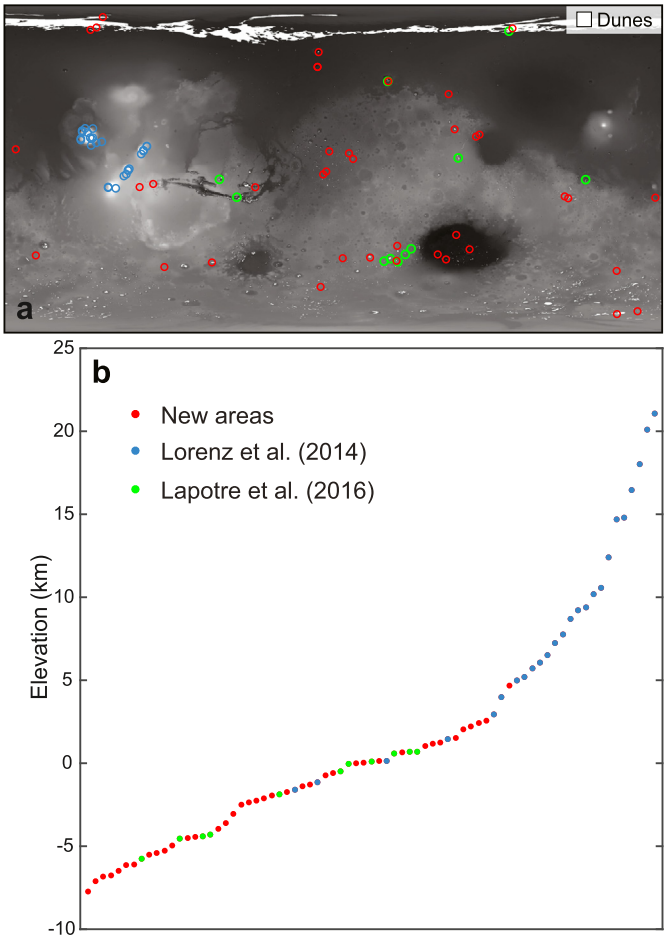

Fig. 1. - Location (a) and elevation distribution (b) of the 75 sites surveyed in this study. We analyzed the same 25 areas (blue) of Lorenz et al. (2014) as well as the 11 dark-tone dune sites (green) previously analyzed by Lapotre et al. (2016). Our survey improves the spatial coverage, extends the range of surveyed elevations and provides a more continuous elevation sampling. A global dune catalog (Hayward et al., 2014; Fenton, 2020) is shown overlaying MOLA elevation data.

methods used to collect the elevation values). In their supplementary materials, Lapotre et al. (2016) mentions that Lorenz's data "were measured with respect to the Mars Reconnaissance Orbiter reference ellipsoid" and that for this reason they have corrected the data to be consistent with the areoid datum used in their survey. We applied the same correction, converting Lorenz's (2014) elevations to orthometric heights.

Previous studies analyzed the relation between the average wavelength and atmospheric density at the surface, focusing on large ripples and TARs. To comply with this framework, we segment the mapped bedforms in two classes: a) large dark-toned ripples and b) a second class that comprises megaripples and TARs. Wavelength and relative grain size were proposed to be key parameters to discriminate different types of aeolian bedforms on Mars (Day and Zimbelman, 2021). We use albedo as a proxy for grain size, as it is usually assumed to be related to dust coating and/or to the presence of coarser particles (Sullivan et al., 2020). We examine the wavelength and albedo distributions using 2D histograms and we define threshold values that allow the partition of the mapping results, so that summary statistics can be computed for each class (see Supplementary material 1 - section S1.3 for examples, Supplementary material 2 for global results and Supplementary material 3 for the compiled database).

To identify possible outliers and evaluate relations between dune morphology and large ripples morphometry, we identified the type of dunes in the areas mapped outside Tharsis (section 3.3), as that region lacks dark dunes. Most areas present more than one dune type, therefore we used a dual classification scheme, visually identifying primary and secondary dune types. Primary class corresponds to the type of dune most abundant, in terms of relative area. To evaluate the mechanisms that set the size of large ripples on Mars we test which model best describes the wavelength vs. atmospheric density relation observed in our dataset. We tested three models (refer to Supplementary material 1 - section S2 for details on the estimation of atmospheric density and models' implementation): a) the wind-drag model of Lapotre et al. (2016), where the saturation length scale is approximated as that of fluvial bedload, b) a modified version of the same scaling, which instead uses a saturation length scale for aeolian saltation (Duran Vinent et al., 2019; Lapotre et al., 2021), and c) a generic inverse linear dependence between wavelength and atmospheric density (as proposed by Lorenz et al., 2014). We fit power laws and linear models to facilitate the comparison between our measurements and the models' predictions.

3. Results and discussion

3.1. Mapping results and comparison with previous studies

Bedforms spaced between 1 to 100 m were mapped over a total area of ~2200 km^2 (Supplementary material 2). The applied method correctly identifies the location of bedforms (93.7% of overall accuracy) and robustly measures their wavelength (we estimate a confidence interval of ±12%, Supplementary material 1 - section S1.2).

When comparing our data with previous surveys, we found a good agreement with large ripple measurements reported by Lapotre et al. (2016), which on average differ by 4±10% (with a maximum difference of 21% for Area 2). If we also consider the standard deviation intervals, we conclude that the two sets of measurements are very similar, presenting overlapping distributions (Fig. 3a). However, the averages for the larger bedforms (megaripples and TARs) reported in the same study are severely underestimated, with an average difference of 84±83% and a maximum of 236% (Fig. 3b).

Focusing in the two areas with larger differences (Areas 6 and 8, Table S2), Lapotre et al. (2016) collected 36 and 40 measurements for TARs and 136 and 98 for large ripples. These were randomly sampled across the HiRISE scenes with dark dunes or other bedforms. Yet, our complete mapping reveals that megaripples/TARs only cover a small fraction of the mapped areas (38 and 20% respectively), in addition they tend to form disperse sets of bedforms with variable wavelengths. Therefore, we hypothesize that undersampling in previous studies is the main reason for the observed wavelength disparities in the case of megaripples/TARs.

Our results for the Tharsis sites (which represent ~2/3 of the data analyzed in (Lapotre et al., 2016)) show that Lorenz et al. (2014) values are systematically underestimated (Fig. 3a): on average they are 73±106% lower than the values obtained in this study (a maximum percentual difference of 563% was measured in Area 55). Indeed, some cited measurements there (e.g., 0.5-1.1 m) are dubious at best given HiRISE resolution (0.25 m/pix). The causes for this large disparity are less clear, nevertheless we note that in this case the measurement locations were not randomized (in each site approximately 40 sets of bedforms were sampled, divided by four selected sub-areas), and that in some of the areas the spatial distribution of the bedforms is not uniform. These two factors may complicate the obtention of representative values from a few tens of scattered measurements.

Other potential sources of uncertainty are the elevation values reported for each site, which are used to derive the atmospheric

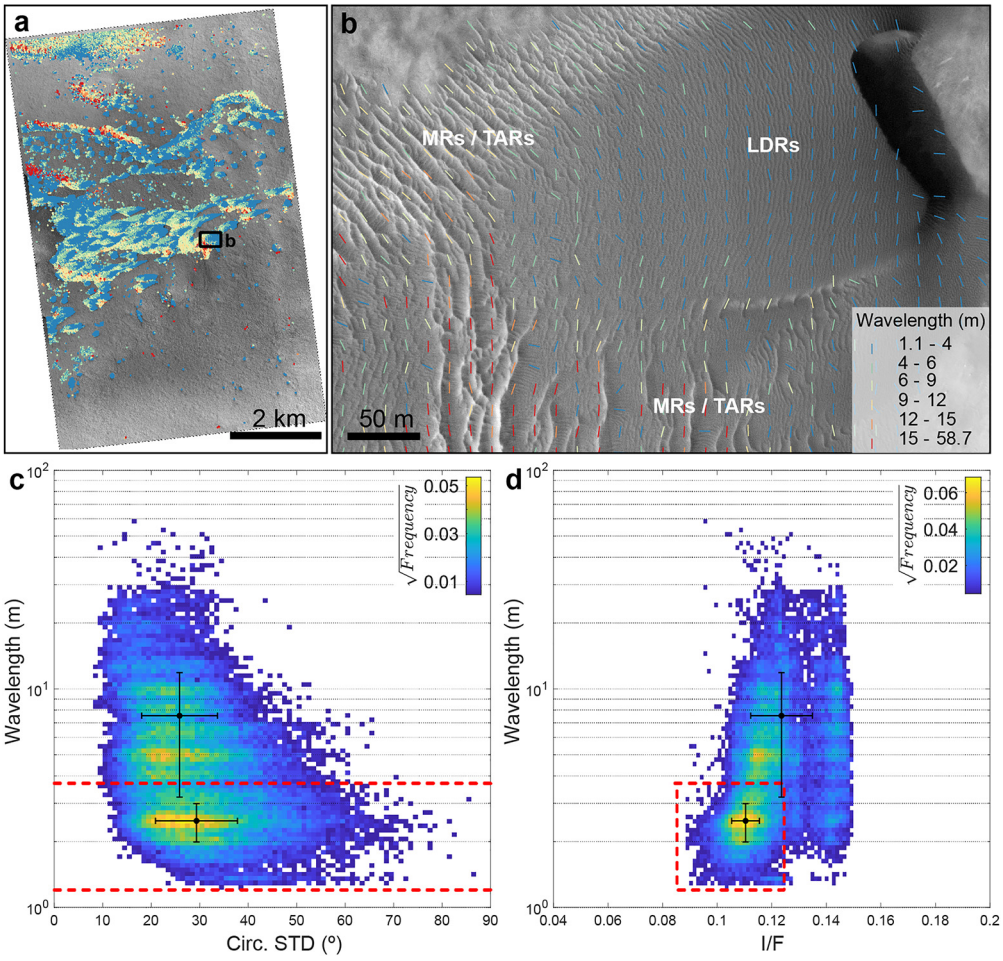

Fig. 2. - Wavelength survey of aeolian bedforms on Lyot crater (ESP_055318_2290, area 26 in Table S1). a) The applied method allows the full mapping and wavelength characterization of aeolian bedforms. Note, transport direction is toward the east. b) Detailed view of the wavelength and trend of the mapped bedforms: large dark-toned ripples (LDRs) cover a barchan dune and have a spacing between crests of less than 4 m; megaripples (MRs) and transverse aeolian ridges (TARs) present higher albedos, higher wavelengths and are overlaid by the dune darker sediments. c and d) 2D histograms showing the distribution of wavelength, circular standard deviation and albedo (I/F), a square root stretch is used to highlight secondary peaks. Red dashed lines correspond to the wavelength and albedo thresholds used to segment two bedform classes. The black dots and lines represent the computed averages and 1σ intervals.

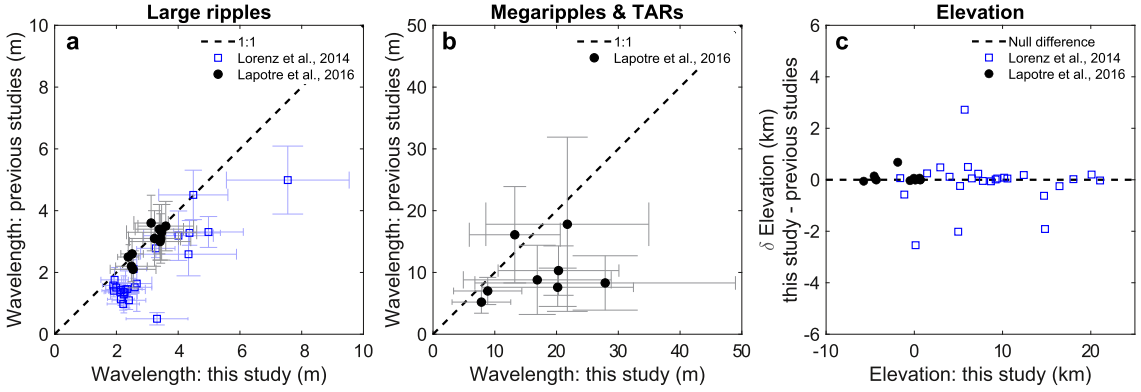

Fig. 3. - Comparison of wavelength and elevation measurements. a) Large ripples: there is a good agreement with Lapotre et al. (2016) values and error bars always overlap the 1:1 (perfect agreement) line; when compared with our data, Lorenz et al. (2014) measurements are clearly underestimated. b) In the case of the larger bedforms, half of Lapotre et al. (2016) values are comparable to our data, while the other half seems to be relatively underestimated (Table S2 presents the percentual differences for each area). c) Lapotre et al. (2016) elevation values are consistent with our work; the differences with Lorenz et al. (2014) measurements are more relevant, with elevation differences that can reach 3 km, which is justified by the fact that high slope areas in the Tharsis region (e.g. Olympus Mons basal scarp) can produce large topographic gradients even inside the relatively small footprint of an HiRISE image.

pressure. As previously mentioned, we sampled the MOLA elevations at the centroid point of the largest bedform patch mapped in each area. However, previous works do not specify the sampling scheme or location where elevation values were collected. Fig. 3c shows the differences in elevations for all mapped areas. We found a good agreement with Lapotre et al. (2016) elevations, the only exception is Area 3, which has an elevation difference of ∼700 m. In this specific case, elevations inside the mapped area can vary by ∼1000 m, therefore the mentioned discrepancy can be attributed to the different sampling location.

Significant differences exist between the elevations computed in this work and part of the elevations reported in Lorenz et al. (2014). In four areas differences can range between 2 and 3 km (Fig. 3c). Also in this case, discrepancies are likely caused by a different sampling location. The Tharsis region extreme topography result in large elevation variations across the HiRISE image footprints. In some cases, maximum elevation differences of ∼4 km are possible, depending where in the image footprint the MOLA data is sampled.

In our study, we implicitly use the location of the mapped bedforms to define the sampling points, thus we adopt a consistent and robust methodology which reduces the uncertainty in the measurement of this variable.

3.2. Investigating the significance of the Tharsis bedforms

To evaluate the wind-drag model predictions, Lapotre et al. (2016) merged their wavelength measurements with the ones derived by Lorenz et al. (2014), for the bedforms located in the Tharsis region. In contrast, a segmentation of the two datasets and the fit of different models was later preferred (Lorenz, 2020; Lapotre et al., 2021). Therefore, the first question we address here is: can we integrate the measurements made in the Tharsis region with others made elsewhere on Mars, or do they constitute different sets of bedforms? To answer this question, we evaluate if there is a unique and continuous distribution of wavelength and albedo. Then we discuss the morphological differences and overall setting and significance of the two sets of bedforms.

In Fig. 4 we compare the wavelength and albedo distributions of the large ripples mapped in the Tharsis region (the same 25 areas of Lorenz et al., 2014) and elsewhere on Mars. The wavelength of Tharsis' bedforms is more variable, on average form more sinuous patterns (i.e. with higher circular standard deviation, Fig. 4a and c) and most importantly, they present higher albedos (Fig. 4b and d). This clearly different albedo signature is further corroborated by plotting the thermal inertias (Putzig and Mellon, 2007) and dust cover index (Ruff and Christensen, 2002) for the mapped areas (Fig. 5). This data shows that the Tharsis bedforms form a distinct population, with lower thermal inertia (possibly denoting finer materials), higher dust coverage/content and morphologies that possess a higher degree of directional variability (the fine "reticulate" texture of the bedforms in this region was previously discussed by Bridges et al., 2010).

The morphology of some of the Tharsis bedforms is also distinctive and variable (e.g. Fig. S2), forming honeycomb patterns or appearing in association with longitudinal spurs/erosive features (Bridges et al., 2010; Lorenz et al., 2014). Tharsis bedforms usually overlay bedrock, forming in some cases extensive mantling units. In contrast, meter-scale bedforms surveyed outside Tharsis typically cover larger scale bedforms (i.e. dark dunes). Tharsis' bedforms were studied in detail by Bridges et al. (2010), proposing that they were formed by saltation of dust aggregates, which in some cases may have produced indurated bedforms. This suggests that major differences in granulometry, density and transport susceptibility exist, and that Tharsis and non-Tharsis bedforms represent two distinct populations.

To summarize, we found several lines of evidence which support that Tharsis bedforms form a distinct population, apart from the large dark-toned ripples found elsewhere on Mars: a) as hinted by Lapotre et al. (2021), we found that Tharsis bedforms have higher albedos; b) we found that they have distinct thermal inertia and dust cover index signatures, denoting lower thermal inertias (possibly associated with finer materials) and higher dust content/coverage; c) as noted by others, Tharsis bedforms form unique patterns (Fig. S2) such as honeycomb or reticulate patterns (Bridges et al., 2010; Lorenz et al., 2014); and d) are in most cases associated with extensive mantling units, while large ripples outside Tharsis are typically found overlaying dark dunes. These distinctive characteristics suggest that the two sets of bedforms should be considered separately when evaluating bedform-formation mechanisms.

3.3. Exploratory data analysis: identification of outliers

Another point we address regards the uniformity of the dataset collected outside Tharsis, does our survey include areas which may not be representative of the global trend, i.e. do we have and can we identify possible outliers? A linear direct relation is evident between average wavelength and elevation (Fig. 6), although a few points deviate from the overall trend (the five labeled points in the plot correspond to the outliers we discuss here). Coincidently, we notice that these five areas have a common attribute: a significant part of the meter-scale bedforms in the areas is located on sand sheets and/or dome dunes.

A closer inspection further revealed other factors that may condition the average measurements for these areas. Namely, in Area 16 (Fig. S3) we have a mixture of two sets of bedforms, one covering barchans and other covering a sand sheet area. The latter set presents lower wavelengths which contribute to lower the average wavelength plotted in Fig. 6, producing a noticeable underestimation. Large ripples in Area 34 (Fig. S4) cover low-lying dome dunes or small sand patches located in depressions. This may justify why this area does not follow the same generic trend, as these topographic settings may shelter bedforms and influence their wavelength. Moreover, the assumption of well sorted sediments may not apply in this case, since substantial lag materials may be present in this sediment starved environment. We also note that large ripples in some of the areas identified as outliers are overprinted by dust devil tracks (Fig. S5). This may denote low or even null migration of the bedforms, since the presence of dust devil tracks implies cycles of dust deposition and removal.

Therefore, five areas stand out as outliers (∼7% of the analyzed areas), corresponding to cases where: a) sand sheets occupy a significant percentage of the mapped areas, suggesting the presence of coarse and/or poorly sorted sediments; and b) where dust devil tracks are visible covering the bedforms, suggesting limited migration/activity and that the ripples present in those areas may not be in equilibrium with present-day atmospheric conditions. These outliers are not included in the fits done to evaluate the proposed models (section 3.4), but their existence highlights two points: the accuracy and consistency of the measurements and the need to select comparable dune settings, as differences in grain size, sorting, and potential activity influence the wavelength of the bedforms.

3.4. Wavelength vs. atmospheric density: model assessment

As discussed, previous surveys were dominated by Tharsis measurements, which are probably biased and correspond to a different type of bedforms. The new data compiled in this work confirms the existence of a decrease of wavelength with increasing atmospheric density for the large dark-toned ripples (Fig. 7). The

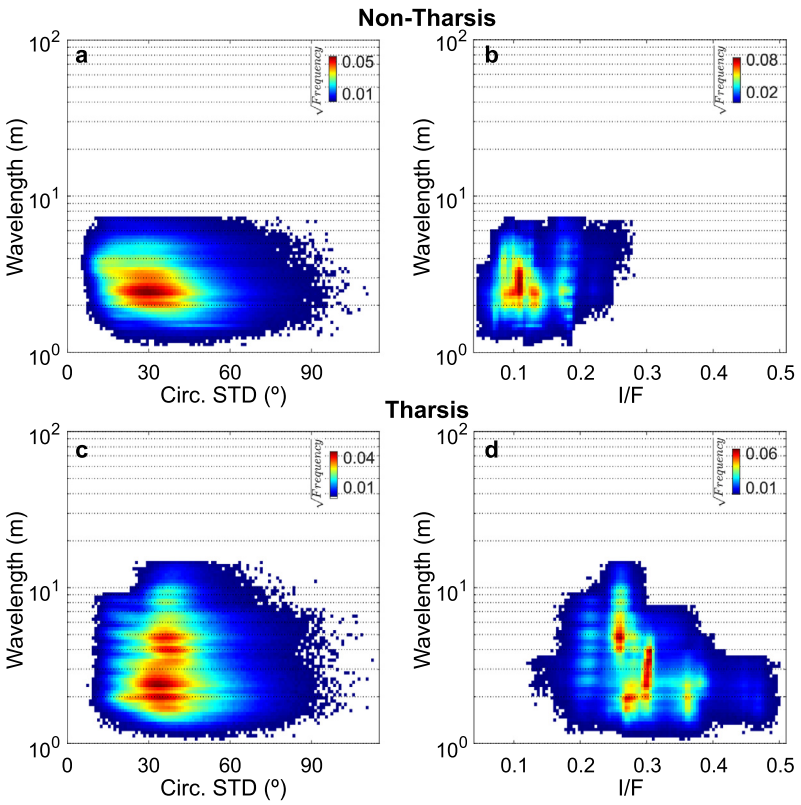

Fig. 4. - 2D histograms of the meter-scale bedforms mapped in the Tharsis region (c, b) and elsewhere on Mars (a, b). Bedforms in Tharsis show a larger dispersion of wavelengths (clustering at ~2.5 m outside Tharsis and ranging from 1.5-5 m in Tharsis), form patterns with larger trend variations (median circular standard deviation of ~30° vs. 30-45°) and consistently present higher albedos (<0.25 vs. >0.2).

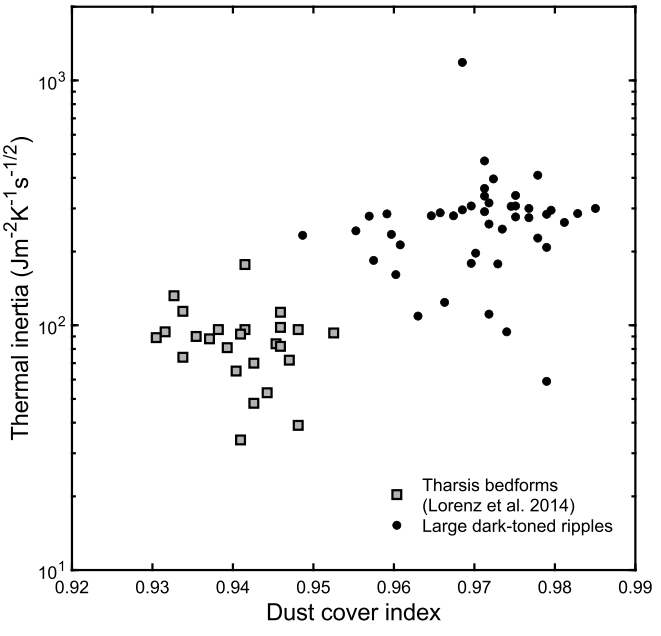

Fig. 5. - Nightside TES thermal inertia (Putzig and Mellon, 2007) vs. dust cover index (Ruff and Christensen, 2002) for all mapped areas. Tharsis areas form a distinct cluster, characterized by lower thermal inertias and lower dust cover index (lower index values are indicative of dust covering, while higher values correspond to dust free areas). This demonstrates that the Tharsis bedforms form a different population, in terms of thermophysical proprieties and dust coverage/content.

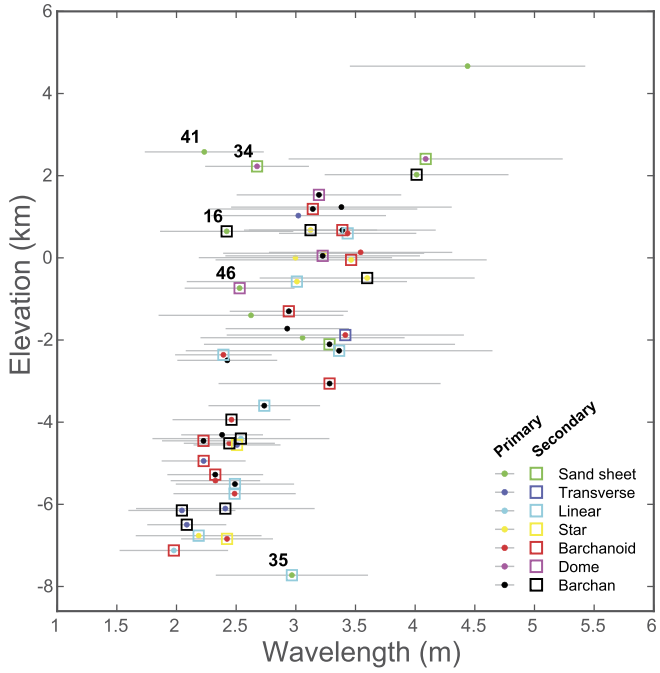

Fig. 6. - Average wavelength vs. elevation for the 50 areas located outside Tharsis, gray lines correspond to 1σ intervals. The color code represents the type of dune morphology present in the mapped areas, when more than one type is present, we assign a primary (covering higher area) and secondary class. The five labeled sites correspond to the outliers discussed in this section.

model obtained by fitting previous datasets which takes into account the bedload transport saturation length (Lapotre et al., 2016) predicts significantly lower wavelengths and a different scaling to the one we derived from our dataset. Conversely, our data for the dark-toned large ripples overlaps the predictions of the wind-drag model that uses the saltation transport saturation length, with a best fitted power law with ~2/3 scaling.

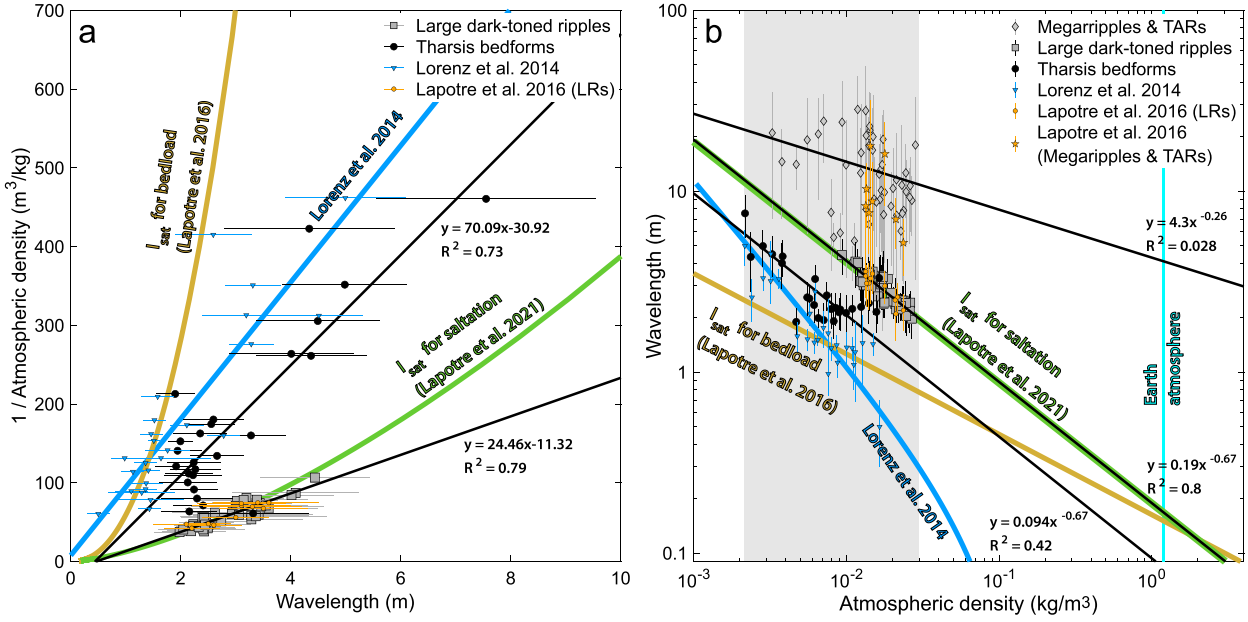

Fig. 7. – Previous surveys and relation between bedforms wavelength and Martian atmospheric density. The same data is shown in two different plots: a) highlighting the linear inverse relation proposed by Lorenz et al. (2014) and b) comparing with the models proposed by Lapotre et al. (2016, 2021), the gray area represents the maximum range of atmospheric densities on Mars while the cyan line represents the density of Earth's atmosphere. Black lines represent the best fitted models for our datasets, computed using the average wavelengths for each site (linear models in a) and power laws in b); the R^2 values in b) were computed in the log space). The blue line corresponds to a linear fit ($\mathbf{1/\rho = 86.8x + 7.7}$; $\boldsymbol{R^2 = 0.75}$) performed using Lorenz et al. (2014) wavelength measurements, here we plot atmospheric densities derived from orthometric elevations, therefore our fit is slightly different from the one presented in Lorenz et al. (2014). The golden line represents Lapotre et al. (2016) empirical relationship where transport saturation length (l_{sat}) is taken as that of fluvial bedload, while the green line corresponds to predictions using a transport saturation length for aeolian saltation (Lapotre et al., 2021). A simplified version of these plots, where the data points from previous studies are omitted, is included in Fig. S14.

Tharsis data presents higher scattering, particularly for lower wavelengths where data points seem to converge towards the dark-toned ripple dataset. Due to the discrepancies found between our results and those of Lorenz et al. (2014), we note that the Tharsis data compiled in this study does not overlap or follow a similar scaling to the wind-drag model that considers a bedload transport saturation length (Fig. 7 and S14). Instead, the best fitted power law ($R^2 = 0.42$) has the same scaling ($\sim$2/3) of the model that uses the saltation transport saturation length.

The compiled data suggests that the mechanism that limits the size of large ripples on Mars is dependent on the atmospheric density. Overall, we observe that all our data are bounded by the two saturation length scaling laws, supporting the hypothesis that the equilibrium size of large martian ripples is controlled by an aerodynamic mechanism. The scaling laws for saturation length arise from idealized representations of transport in unimodal sediments. As previously discussed, the grain size distribution of the sediments on the Tharsis bedforms is probably more complex, which may contribute to the observed differences between Tharsis and non-Tharsis bedforms.

Even so, in accordance with previous studies (Lorenz et al., 2014; Lorenz, 2020) we notice that linear functions (which imply that $\lambda \propto 1/\rho_f$) also provide robust fits to the data ($R^2 = 0.79$ and 0.73 for the dark large ripples and Tharsis bedforms, respectively). In the case of the large ripples, both inverse and power law functions explain $\sim$80% of the variance. This means that, strictly from a numeric point of view, we cannot discriminate what is the best model to fit the data. As previously mentioned, to fully test the impact ripple hypothesis we would need to consider the wind velocities at each site, something that could be done using climate model predictions. Yet, we note that Rubanenko et al. (2022) compared hypsometric densities (like used in this study) with GCM-derived atmospheric densities and shear velocities, concluding that the $\sim$2/3 scaling also applies to the GCM predictions (supporting the hydrodynamic anomaly hypothesis). A similar analysis for the sites where we measure the wavelength of dark-toned ripples may reveal the same trend, helping to test and constrain the suitability of the models.

Finally, the wavelengths of the larger bedforms (megaripples and TARs) present a large dispersion (Fig. 7b), not showing an obvious relation with any of the scaling laws. Linear or power law models do not produce a meaningful fit to the data ($R^2 = 0.03$). This suggests that at a global scale these bedforms do not form a homogeneous set and are probably not representative of the same boundary conditions (i.e., they likely formed with different grain size distributions, or under differing atmospheric conditions). Nonetheless, we cannot exclude the possibility that including TARs and megaripples in a same class may be flawed, especially since different degrees of mobility under present day winds have been described for the two sets of bedforms (Silvestro et al., 2020; Chojnacki et al., 2021).

For the dark-toned large ripples the degree of agreement between the global measurements and the predictions of the scaling relationship of Lapotre et al. (2021) (where saturation length is taken as that of aeolian saltation) is remarkable. Particularly if we consider that we are using a "static" average atmospheric density, which is merely a function of elevation and does not consider regional and seasonal atmospheric density variations. On the other hand, we cannot exclude that the density may just be one of the factors influencing the bedforms dimensions. As suggested by Lorenz (2020), wind speed at a global scale may increase with elevation creating a more complex interplay between density, wind speed and resulting bedform size.

4. Conclusions

This survey provides improved measurements to evaluate the mechanisms that set the size of bedform on Mars. We show that previous works used biased measurements, particularly for the bedforms located in the Tharsis region. We investigated the

uniqueness of the bedforms located in this region, concluding that these bedforms form a distinct population and should be analyzed separately from the more common dark-toned large ripples that cover dunes outside Tharsis.

Our survey covers a larger range of elevations than previous works, and for the first time provides full wavelength mapping of extensive regions. Overall, our results are consistent with the predictions of the "wind-drag" hypothesis, favoring the model that considers a saltation transport saturation length. Rubanenko et al. (2022) presented other evidence that supports this hypothesis: the size of small dunes also decreases with density, following a similar ∼2/3 scaling; and the existence of a wavelength gap between large ripples and small dunes. Still, solely the compiled morphometric data in this study is not enough to refute the impact ripple hypothesis, as that would probably require the integration of variable wind velocities for each site.

The compiled dataset corroborates the existence of a robust relation between the wavelength of meter-scale bedforms and atmospheric density, as firstly reported by Lorenz et al. (2014). This new survey complements and helps to validate the main concept introduced in Lapotre et al. (2016): that paleo-atmospheric density can be inferred for Mars by looking at the aeolian sedimentary record, providing an important tool to probe the evolution of the planet's environment (e.g. Rubin et al., 2022). The significative differences we found for the Tharsis bedforms underscore that a careful sedimentological analysis of paleobedforms is necessary, as grain size and dust content may influence their wavelength. Therefore, paleo-atmospheric inferences should preferentially target remnant bedforms sedimentologically akin to present-day large dark-toned ripples, a type of bedforms for which the obtained wavelength vs. atmospheric density relation is better constrained.

CRediT authorship contribution statement

David A. Vaz: Conceptualization, Investigation, Methodology, Software development, Writing – original draft.

S. Silvestro: Conceptualization, Investigation, Writing – original draft, Writing – review & editing.

Matthew Chojnacki: Investigation, Writing – original draft, Writing – review & editing.

David C. A. Silva: Validation, Visualization, Writing – review & editing.

Declaration of competing interest

The authors declare that they have no known competing financial interests or personal relationships that could have appeared to influence the work reported in this paper.

Data availability

HiRISE images used in this work are publicly available at the Planetary Data System (https://hirise-pds.lpl.arizona.edu/PDS/) where details can be obtained at McEwen et al. (2007). The morphometric database compiled in this study is provided in Supplementary material 3.

Acknowledgements

This research was supported by CITEUC (UID/Multi/00611/2021&POCI-01- 0145-FEDER-006922) and by Fundação para a Ciência e a Tecnologia (FCT) grant CEECIND/02981/2017. M. C. and S.S. were funded by NASA Mars Data Analysis Program Grant 80NSSC20K1066. We thank the Laboratory for Advanced Computing at University of Coimbra for providing computing resources.

We acknowledge the valuable comments and suggestions made by Ralph Lorenz, Mathieu Lapotre and two anonymous reviewers to an earlier version of this work. We thank Rob Sullivan for discussion and insights on the morphodynamics of impact ripples.

Appendix A. Supplementary material

Supplementary material related to this article can be found online at https://doi.org/10.1016/j.epsl.2023.118196.

References

Andreotti, B., Claudin, P., Iversen, J.J., Merrison, J.P., Rasmussen, K.R., 2021. A lower-than-expected saltation threshold at Martian pressure and below. Proc. Natl. Acad. Sci. USA 118. https://doi.org/10.1073/pnas.2012386118.

Andreotti, B., Claudin, P., Pouliquen, O., 2006. Aeolian sand ripples: experimental study of fully developed states. Phys. Rev. Lett. 96. https://doi.org/10.1103/Physrevlett.96.028001.

Bagnold, R.A., 1941. The Physics of Blown Sand and Desert Dunes. Methuen, London. 265 p.

Baker, M.M., Lapotre, M.G.A., Minitti, M.E., Newman, C.E., Sullivan, R., Weitz, C.M., Rubin, D.M., Vasavada, A.R., Bridges, N.T., Lewis, K.W., 2018. The Bagnold Dunes in southern summer: active sediment transport on Mars observed by the curiosity rover. Geophys. Res. Lett. 45, 8853–8863. https://doi.org/10.1029/2018GL079040.

Baker, M.M., Newman, C.E., Sullivan, R., Minitti, M.E., Edgett, K.S., Fey, D., Ellison, D., Lewis, K.W., 2022. Diurnal variability in aeolian sediment transport at Gale crater, Mars. J. Geophys. Res., Planets 127, 1–27. https://doi.org/10.1029/2020JE006734.

Bridges, N.T., et al., 2010. Aeolian bedforms, yardangs, and indurated surfaces in the Tharsis Montes as seen by the HiRISE Camera: evidence for dust aggregates. Icarus 205, 165–182. https://doi.org/10.1016/j.icarus.2009.05.017.

Bridges, N.T., Ayoub, F., Avouac, J.-P., Leprince, S., Lucas, a, Mattson, S., 2012. Earth-like sand fluxes on Mars. Nature 485, 339–342. https://doi.org/10.1038/nature11022.

Cheng, H., Liu, C., Li, J., Liu, B., Zheng, Z., Zou, X., Kang, L., Fang, Y., 2018. Experimental study of aeolian sand ripples in a wind tunnel. Earth Surf. Process. Landf. 43, 312–321. https://doi.org/10.1002/esp.4246.

Chojnacki, M., Vaz, D.A., Silvestro, S., Silva, D.C.A., 2021. Widespread megaripple activity across the North polar ergs of Mars. J. Geophys. Res., Planets, 1–19. https://doi.org/10.1029/2021je006970.

Day, M., Zimbelman, J.R., 2021. Ripples, megaripples, and TARs, Oh, My! Recommendations regarding Mars aeolian bedform terminology. Icarus 369, 114647. https://doi.org/10.1016/j.icarus.2021.114647.

Duran Vinent, O., Andreotti, B., Claudin, P., Winter, C., 2019. A unified model of ripples and dunes in water and planetary environments. Nat. Geosci. 12, 345–350. https://doi.org/10.1038/s41561-019-0336-4.

Fenton, L.K., 2020. Updating the global inventory of dune fields on Mars and identification of many small dune fields. Icarus 352, 114018. https://doi.org/10.1016/j.icarus.2020.114018.

Foroutan, M., Zimbelman, J.R., 2017. Semi-automatic mapping of linear-trending bedforms using 'Self-Organizing Maps' algorithm. Geomorphology 293, 156–166. https://doi.org/10.1016/j.geomorph.2017.05.016.

Gough, T.R., Hugenholtz, C.H., Barchyn, T.E., 2021. Re-evaluation of large Martian ripples in Gale crater: granulometric evidence for an impact mechanism and terrestrial analogues. J. Geophys. Res., Planets 126. https://doi.org/10.1029/2021JE007011.

Hayward, R.K., Fenton, L.K., Titus, T.N., 2014. Mars global digital dune database (MGD3): global dune distribution and wind pattern observations. Icarus 230, 38–46. https://doi.org/10.1016/j.icarus.2013.04.011.

Lapotre, M.G.A., et al., 2016. Large wind ripples on Mars: a record of atmospheric evolution. Science 353, 55–58. https://doi.org/10.1126/science.aaf3206.

Lapotre, M.G.A., Ewing, R.C., Lamb, M.P., 2021. An evolving understanding of enigmatic large ripples on Mars. J. Geophys. Res., Planets 126, 1–8. https://doi.org/10.1029/2020JE006729.

Lapotre, M.G.A., Ewing, R.C., Weitz, C.M., Lewis, K.W., Lamb, M.P., Ehlmann, B.L., Rubin, D.M., 2018. Morphologic diversity of Martian ripples: implications for large-ripple formation. Geophys. Res. Lett. 45, 10,229–10,239. https://doi.org/10.1029/2018GL079029.

Lapotre, M.G.A., Lamb, M.P., McElroy, B., 2017. What sets the size of current ripples? Geology 45, G38598.1. https://doi.org/10.1130/G38598.1.

Lorenz, R.D., 2020. Martian ripples making a splash. J. Geophys. Res., Planets 125, 12–15. https://doi.org/10.1029/2020JE006658.

Lorenz, R.D., Bridges, N.T., Rosenthal, A.A., Donkor, E., 2014. Elevation dependence of bedform wavelength on Tharsis Montes, Mars: atmospheric density as a controlling parameter. Icarus 230, 77–80. https://doi.org/10.1016/j.icarus.2013.10.026.

Manukyan, E., Prigozhin, L., 2009. Formation of aeolian ripples and sand sorting. Phys. Rev. E, Stat. Nonlinear Soft Matter Phys. 79. https://doi.org/10.1103/PhysRevE.79.031303.

McEwen, A.S., et al., 2007. Mars reconnaissance orbiter's high resolution imaging science experiment (HiRISE). J. Geophys. Res., Planets 112. https://doi.org/10.1029/2005je002605.

Putzig, N.E., Mellon, M.T., 2007. Apparent thermal inertia and the surface heterogeneity of Mars. Icarus 191, 68–94. https://doi.org/10.1016/j.icarus.2007.05.013.

Rasmussen, K.R., Valance, A., Merrison, J., 2015. Laboratory studies of aeolian sediment transport processes on planetary surfaces. Geomorphology 244, 74–94. https://doi.org/10.1016/j.geomorph.2015.03.041.

Rubanenko, L., Lapôtre, M.G.A., Ewing, R.C., Fenton, L.K., Gunn, A., 2022. A distinct ripple-formation regime on Mars revealed by the morphometrics of barchan dunes. Nat. Commun. 13, 1–7. https://doi.org/10.1038/s41467-022-34974-3.

Rubin, D.M., et al., 2022. Ancient winds, waves, and atmosphere in Gale crater, Mars, inferred from sedimentary structures and wave modeling. J. Geophys. Res., Planets 127, 1–23. https://doi.org/10.1029/2021JE007162.

Ruff, S.W., Christensen, P.R., 2002. Bright and dark regions on Mars: particle size and mineralogical characteristics based on thermal emission spectrometer data. J. Geophys. Res. E, Planets 107, 1–22. https://doi.org/10.1029/2001je001580.

Sharp, R.P., 1963. Wind ripples. J. Geol. 71, 617–636. http://www.jstor.org/stable/30061128.

Silvestro, S., Chojnacki, M., Vaz, D.A., Cardinale, M., Yizhaq, H., Esposito, F., 2020. Megaripple migration on Mars. J. Geophys. Res., Planets 125. https://doi.org/10.1029/2020JE006446.

Silvestro, S., Fenton, L.K., Vaz, D.A., Bridges, N.T., Ori, G.G., 2010. Ripple migration and dune activity on Mars: evidence for dynamic wind processes. Geophys. Res. Lett. 37, L20203. https://doi.org/10.1029/2010gl044743.

Silvestro, S., Vaz, D.A., Ewing, R.C., Rossi, A.P., Fenton, L.K., Michaels, T.I., Flahaut, J., Geissler, P.E., 2013. Pervasive aeolian activity along rover curiosity's traverse in Gale crater, Mars. Geology 41, 483–486. https://doi.org/10.1130/G34162.1.

Silvestro, S., Vaz, D.A., Yizhaq, H., Esposito, F., 2016. Dune-like dynamic of Martian Aeolian large ripples. Geophys. Res. Lett. 43, 8384–8389. https://doi.org/10.1002/2016GL070014.

Smith, D.E., et al., 1999. The global topography of Mars and implications for surface evolution. Science 284, 1495–1503.

Sullivan, R., Baker, M., Newman, C., Turner, M., Schieber, J., Weitz, C., Hallet, B., Ellison, D., Minitti, M., 2022. The aeolian environment in Glen Torridon, Gale crater, Mars. J. Geophys. Res., Planets 127, 1–39. https://doi.org/10.1029/2021JE007174.

Sullivan, R., Kok, J.F., 2017. Aeolian saltation on Mars at low wind speeds. J. Geophys. Res., Planets 122, 2111–2143. https://doi.org/10.1002/2017JE005275.

Sullivan, R., Kok, J.F., Katra, I., Yizhaq, H., 2020. A broad continuum of aeolian impact ripple morphologies on Mars is enabled by low wind dynamic pressures. J. Geophys. Res., Planets 125, 1–39. https://doi.org/10.1029/2020je006485.

Swann, C., Sherman, D.J., Ewing, R.C., 2020. Experimentally derived thresholds for windblown sand on Mars. Geophys. Res. Lett. 47, 1–10. https://doi.org/10.1029/2019GL084484.

Vaz, D.A., Silvestro, S., 2014. Mapping and characterization of small-scale aeolian structures on Mars: an example from the MSL landing site in Gale crater. Icarus 230, 151–161.

Vaz, D.A., Silvestro, S., Sarmento, P.T.K., Cardinale, M., 2017. Migrating meter-scale bedforms on Martian dark dunes: are terrestrial aeolian ripples good analogues? Aeolian Res. 26, 101–116. https://doi.org/10.1016/j.aeolia.2016.08.003.

Voulgaris, G., Morin, J.P., 2008. A long-term real time sea bed morphology evolution system in the South Atlantic Bight. In: Proceedings of the Ieee/Oes/Cmtc Ninth Working Conference on Current Measurement Technology, pp. 71–79.

Weitz, C.M., Sullivan, R.J., Lapotre, M.G.A., Rowland, S.K., Grant, J.A., Baker, M., Yingst, R.A., 2018. Sand grain sizes and shapes in eolian bedforms at Gale crater, Mars. Geophys. Res. Lett. 45, 9471–9479. https://doi.org/10.1029/2018GL078972.